Structures and phase transitions of amorphous ices

Ichiro Okabe and Hideki Tanaka
Division of Polymer Chemistry, Graduate School of Engineering, Kyoto University, Sakyo, Kyoto 606-01, Japan

Koichiro Nakanishi
Department of Chemical Technology, Kurashiki University of Science and the Arts, Nishinoura 2640, Tsurajimacho, Kurashiki, Okayama 712, Japan

(Received 29 August 1995)

Molecular dynamics simulations have been carried out in order to clarify the structural and hydrogen bond network differences among high density amorphous ice (HDA), low density amorphous ice (LDA), and hexagonal ice (ice I_h). Ice I_h is transformed to HDA at 1.27 GPa and 77 K. A very long time (order of a nanosecond) to complete the transition is required. It is found that molecular motions are delocalized in the early stage and become localized in the final stage of the relaxation. LDA is obtained by heating HDA to 160 K. The second peak of the radial distribution function is more clearly separated from the first peak in LDA than in HDA. Few bifurcated hydrogen bonds are found in LDA compared with HDA, which is evidence that LDA resembles crystal ice in short range order. The network topology of the system is also analyzed in terms of the distribution of Voronoi polyhedra, where the density lies between stable HDA and LDA. Density fluctuations are found, which should be attributed to the precursor of a phase separation between HDA and LDA.

PACS number(s): 64.70.Kb, 64.60.−i

I. INTRODUCTION

Water is one of the most ubiquitous substances on Earth and exhibits various anomalous properties such as the density maximum temperature [1]. Its solid phase has a rich variety of polymorphs [2]. It is also believed that at least two metastable phases of amorphous ices exist [3]; they are referred to as low density amorphous ice (LDA) and high density amorphous ice (HDA). The phase diagram for these amorphous ices including the supercooled liquid state is still controversial.

Speedy and Angell [4] accounted for the divergence of thermodynamic properties in a supercooled state in conjunction with the liquid-vapor spinodal. The liquid spinodal line is the limit of mechanical stability of the liquid state with respect to fluctuations toward a thermodynamically stable phase. The liquid spinodal line begins at the liquid-gas critical point. In the plane of pressure P and the temperature T, this line decreases monotonically with decreasing T along a path lying below the liquid-gas coexistence curve. Speedy and Angell [4] conjectured that the liquid spinodal line of water in the pressure-temperature plane does not decrease monotonically with decreasing temperature. Speedy [5] proposed the stability-limit conjecture; the liquid spinodal line has a minimum at negative pressure and passes back to positive pressure as the temperature decreases further. The increasingly anomalous thermodynamic behavior of liquid water in the low temperature region can be interpreted via such a reentrant spinodal line.

The conjectured minimum in the liquid spinodal line has not been directly observed due to the experimental difficulties. Poole *et al.* [6] carried out molecular dynamics simulations over a wide range of stable, metastable, and unstable liquid-state points, and demonstrated that the liquid spinodal line does not reenter into the positive P region. Rather, the anomalies are related to the critical point from which the LDA-HDA phase boundary appears.

In order to model the phase behavior of liquid water, Poole *et al.* [7] developed a van der Waals type equation. In their model, the free energy is separated into two parts, the van der Waals free energy and the free energy due to hydrogen bonds, both of which are functions of the volume and have minima at fairly different molar volumes. This model with appropriate parameters predicts, though qualitatively, anomalous thermodynamic properties of water, such as density maximum temperature, the divergence in the compressibility, and the heat capacity. At sufficiently low temperature, the free energy in this model has two minima. They associated the LDA↔HDA transition with the transition from a free energy local minimum to another in the density coordinate axis. However, this model also yields a different phase diagram by a slight change of the parameters.

LDA can be prepared not by normal cooling but by the following methods: (1) deposit vapor onto a cold plate or hyperquench liquid state [8], (2) project a thin jet of liquid water at high speed into liquid nitrogen (Mayer *et al.* [9]), (3) ultraviolet irradiation on cubic ice (ice I_c) under 70 K (Kouchi *et al.* [10]). Mishima *et al.* invented the other way to make amorphous water [3]. They compressed hexagonal ice (ice I_h) at 77 K to its extrapolated melting point of 1 GPa. Since the fluid is well below the glass transition at the melting point, it remains in an amorphous state after the pressure is recovered to 0 Pa. They call this phase high density amorphous ice (HDA). The density of HDA is $\sim$1.17 g/cm^3. On heating at zero pressure, HDA transforms at $\sim$117 K to another

amorphous phase with evolution of heat and the density becomes ~0.95 g/cm^3 [11], which is called low density amorphous ice (LDA). Ice VIII also transforms to LDA analogous to the transition from ice I_h to HDA in the sense that these transitions occur at the extrapolated melting points, when the pressure is removed at about 130 K (Klug *et al.* [12]).

At ~145 K, LDA transforms to ice I_c with heat evolution. At 77 K and ~0.6 GPa LDA is compressed to HDA [13]. The pressure-induced reversible LDA↔HDA transition at about 130–150 K was also reported [14]. Such an apparent first-order phase transition of one amorphous phase of materials other than water to another with a large increase in density has not been reported to the best of our knowledge, although gradual densification of amorphous phases up to 20%, when squeezed to ~10 GPa, has been reported [15].

Whalley and Floriano discussed the entropy change and transition pressure of pressure induced transformation from ice I_h to HDA [16,17]. According to their discussion, the equilibrium pressure between ice I_h and HDA must be about 0.5 GPa, which is about half of the actual transformation pressure. Thus the transformation is limited by the kinetics, not by the thermodynamics, because the transformation occurs at low temperature.

Many kinds of measurements have been reported on pressure-induced amorphous ices. Klug *et al.* estimated the distributions of hydrogen-bonded O—H···O and O—D···O distances using an experimental curve of the O—H stretching frequency as a function of the O—O distance [18]. The most probable bond length in HDA is 2.83 Å and the distribution of bond lengths has a half-width of 0.19 Å. In LDA, the most probable distance decreases to 2.76 Å and the half-width also decreases to 0.09 Å. The most probable O···O distance in ice I_h is 2.75 Å. Bosio *et al.* performed x-ray diffraction measurements of two amorphous ices at atmospheric pressure. They observed that the main differences between HDA and LDA appeared at the second and third neighbors. This corresponds to a distortion of the O—O—O angles out of the ideal tetrahedral value of 109° [19].

Molecular dynamics (MD) simulations of two forms of amorphous solid water have been executed by some authors [20–22]. They showed that the simulation results could reproduce experimental data. Poole *et al.* proposed a phase diagram describing amorphous solid water consistent with the available experimental data [6].

In the present work, we investigate the structural difference between HDA, LDA, and liquid water by performing long time MD simulations. The density fluctuation near the transition point between HDA and LDA is also analyzed. Section II describes the parameters and methods used in MD simulations and analyses. In Sec. III, the results are presented. The conclusions are given in Sec. IV.

II. SIMULATION PROTOCOL

We first prepare an ice I_h configuration which consists of 360 water molecules in a rectangular box. Hydrogen atoms are placed according to Bernal-Flower rules [23]. In order to have an MD cell which has zero dipole moment, the positions of protons are permutated until the total dipole has a vanishing value. In the present simulation, pairwise additivity of all the interactions is postulated. The water-water intermolecular interaction is described by a transferable intermolecular potential with three charge points (TIP4P) [24]. This potential has often been used in the study of water. It is believed to be one of the most reliable potentials. The interaction potentials for all pairs of molecules are truncated smoothly at 8.655 Å. The damping is used for convenience of later analyses. MD simulations are performed in the framework of constant pressure-constant temperature (N,P,T) ensemble. A time step for integration of equations of motion is 0.5 fs. Temperature and pressure are controlled by the Nosé-Andersen method [25,26].

A. Structure analysis

The potential energy surface for a system with many particles has a huge number of potential wells which are proportional to the exponential of N, number of particles in the system. A minimum-energy configuration corresponding to the potential energy well is called an "inherent structure" [27]. In order to analyze dynamics of water, an instantaneous MD configuration (I structure) is often used. I structure can be separated into two elements, a fundamental structure (inherent structure) and an intermolecular vibrational displacement (libration and fast translation) from the inherent structure. Since vibrational displacements are removed in inherent structures, the hydrogen bond network pattern of liquid water is more clearly defined than in I structures [1].

We invoke two ways to extract a fundamental structure. The first way is to quench the I structure. Quenching of the system is a mapping of instantaneous configurations onto the local minimum of the potential energy surface. Quenching is performed using the steepest descent method. We call the inherent structure thus obtained the Q structure. The second way is coarse graining. Coarse graining is performed according to

$$\bar{\boldsymbol{r}}_i(t) = \int_{-\Delta\tau/2}^{\Delta\tau/2} g(t')\boldsymbol{r}_i(t+t')dt', \tag{1}$$

$$g(t') = \alpha \frac{\sin(2\pi t'/\Delta\tau)}{2\pi t'/\Delta\tau}, \tag{2}$$

where $\boldsymbol{r}_i(t)$ is the coordinate (both translational and orientational) of the ith molecule at time t and $\bar{\boldsymbol{r}}_i(t)$ is the averaged coordinate over $\Delta\tau$ (=400 ns) [28]. The coarse-graining operation can also remove the fast intermolecular vibrations. The structure is called the V structure (vibrationally averaged structure) [29].

We define two water molecules as a neighboring pair when the O—O distance is less than 3.5 Å. When the pair interaction energy is lower than –12.0 kJ/mol, it is regarded as a hydrogen bonded pair. A proton, which

is the closest to a hydrogen-bonded oxygen atom partner, is considered to take part in the hydrogen bond. If an proton has two neighbor pairs whose interaction energies are lower than –6.0 kJ/mol, the proton is considered to belong to a bifurcated hydrogen bond (BB_H). If an oxygen atom belongs to more than two pairs whose interaction energy is lower than –6.0 kJ/mol, the oxygen also belongs to another kind of bifurcated hydrogen bond (BB_O).

B. Normal mode analysis

As the simulation temperature is well below the melting point, the system is considered to be solidlike. The probability of transitions per unit time from a potential well to another becomes much lower in amorphous solid than in liquid water. Then normal mode analysis is of some utility. Normal mode analysis is performed by diagonalizing the mass weighted force constant matrix, $\mathbf{m}^{-1/2}\mathbf{V}\mathbf{m}^{-1/2}$, where $\mathbf{V}$ is the second derivative of the intermolecular interaction and $\mathbf{m}$ stands for the mass tensor. In this analysis, the potential energy is expanded as a power series of the particle displacements and is truncated at the quadratic order. The density of state for intermolecular vibrational motions $\rho(\omega)$ can be obtained from an appropriate average over the generated structures. In the case of water, density of state can be roughly divided into three regions. The region above 500 cm^{-1} corresponds almost exclusively to rotational motions of individual molecules. The region between 0 and 400 cm^{-1} corresponds to translational motions [30]. The last region consists of modes which have imaginary frequencies (negative eigenvalues). These modes are unstable modes. For presentational convenience, we plot the imaginary (unstable) frequency modes along the negative frequency region.

C. Voronoi polyhedra analysis

Radial distribution functions (RDF) provide only one-dimensional structural information. Voronoi polyhedron (VP) gives alternative information on coordination structure. If the nearest particle of an arbitrary point in the simulation cell is the ith molecule, this point is considered to be in the VP of the ith particle. In order to characterize the shape of VPs, Ruocco introduced a dimensionless parameter, which is called "asphericity" [31],

$$\eta = \frac{S^3}{36\pi V^2}, \tag{3}$$

where S and V is the face area and the volume of a VP. By definition, η is 1 for a sphere, whereas it equals 1.33, 1.35, and 1.91 for a truncated octahedron, a rhombic dodecahedron, and a cube, respectively. They correspond to the Wigner-Seitz cells of bcc, fcc, and simple cubic (sc) lattices. The asphericity for ice I_h is 2.25, which is due to the tetrahedral arrangement of the first neighbors. In the case of perfect tetrahedron, η is 3.31.

III. RESULTS AND DISCUSSION

A. From ice I_h to HDA

The simulation process is shown in Fig. 1. The pressure is increased at the rate of 4 MPa/ps up to 1.0 GPa. The rate of the pressure increase is 2 MPa/ps between 1.0 GPa and 1.27 GPa. It is found that when ice I_h is compressed to the pressure of 1.27 GPa at 77 K, a new phase of density 1.37 g/cm^3 (between ice I_h and state point A in Fig. 1) is formed. Figure 2 shows the time evolution of potential energies (for the I structure and Q structure) and density between A and C. This transition happens suddenly as is shown in Fig. 2: a sudden increase in the potential energy at about time $t = 200$ ps. The transition is accompanied by a 1.75 kJ/mol increase in potential energy and by a 0.24 g/cm^3 increase in density. This simulation is continued for 3100 ps after the pressure is set to 1.27 GPa and we arrive at the state point C. The data for A (C) are given by averaging over 10 configurations between 600 and 650 ps (3000 ps and 3100 ps) after the pressure is set to 1.27 GPa. Some small and stepwise decreases are seen in the potential energy of the I structure. On the other hand, the density increases abruptly only once at 1200 ps. From A to C, the potential energies of the I structure and Q structure decrease by 0.5 kJ/mol and 0.6 kJ/mol, respectively. The pressure-induced structural change is so slow that 3 ns is required to complete the relaxation. The potential energy of each state point is given in Table I.

Rings made by hydrogen bonded water molecules are enumerated in order to examine a relation between the density and the hydrogen bond network pattern. Table I lists the averaged numbers of rings which consist of 3 to 10 hydrogen bonded water molecules in various conditions ($A \sim H$). Ice I_h consists of 720 6-membered rings only. On the other hand, amorphous ices have a variety of

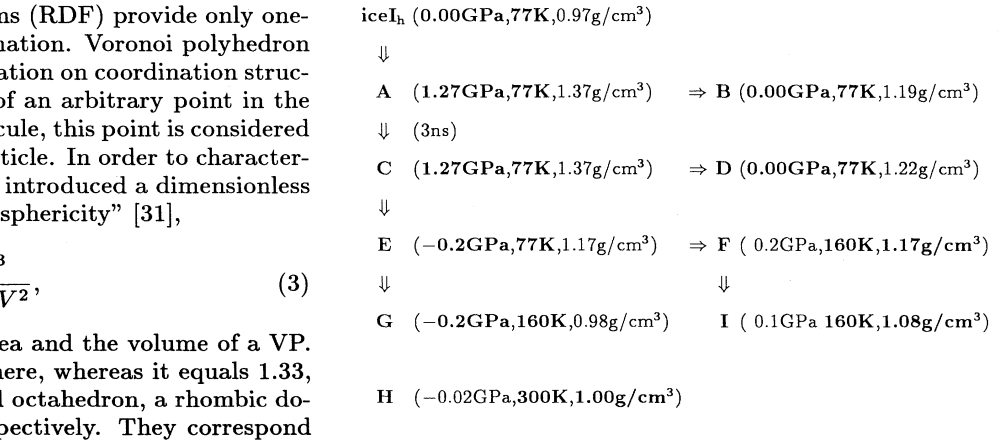

FIG. 1. Simulation process. Bold type means a control parameter. System H, which is liquid water at room temperature, is simulated separately.

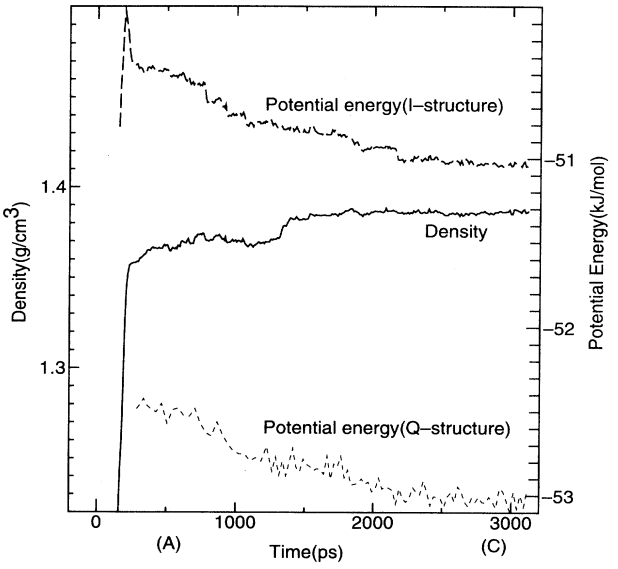

FIG. 2. Potential energies at 77 K and 1.27 GPa in I (thick dashed line) and Q structures (thin dotted line) and density (solid line) of amorphous ice along the trajectory. The curves are coarse grained.

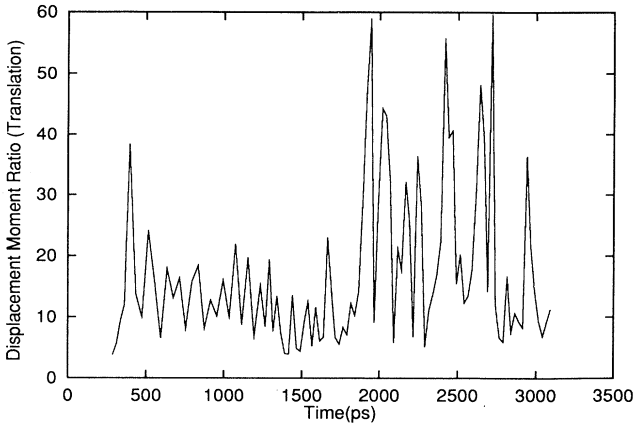

FIG. 3. Time evolution of displaced moment ratio between A and C. Only translational displacements are included. See text.

rings. After long time relaxation (3000 ps), the numbers of 3- to 6-membered rings decrease and those of 7 and 8 rings increase. Especially, the number of 6-membered rings decreases drastically. It means that the topological connectivity of ice I_h still remains at A and the rotational relaxation occurring between A and C changes the connectivity of hydrogen bond network. The ring distributions for B (D) are given by averaging 10 configurations between 90 and 100 ps after the pressure is recovered to 0.0 GPa from A (C). The numbers of 5- and 6-membered rings in A (B) are larger than that in C (D). It shows that the effect of long time relaxation between A and C does not vanish by removing the pressure to 0.0 GPa. In ice VII, 6-membered rings penetrate each other. In the case of A and C, however, either penetration of ring or crossing of hydrogen bonds is not observed. Instead, a high density phase is made by bending hydrogen bonds not by crossing the rings of hydrogen bonds.

The relaxation process in the Q structure is composed only of transitions between adjacent Q structures in configuration space. Individual transitions are expected to be collective in nature as in liquid water [32]. The cooperativity can be quantified by evaluating the displacement moment ratio

$$\xi_d = \frac{(1/N)\sum_{i=1}^{N} \Delta R_i^4}{\left[(1/N)\sum_{i=1}^{N} \Delta R_i^2\right]^2}, \tag{4}$$

where ΔR_i is the molecular displacement of the ith water molecule between two minima, which are separated by 25 ps. Let us consider the case when ΔR takes only 1 or 0. If ΔR of m particles are 1 and the others are 0, ξ_d is

$$\xi_d = \frac{m/N}{(m/N)^2} = \frac{N}{m}. \tag{5}$$

TABLE I. Potential energy and ring size distributions. Conditions for the systems A–H are given in Fig. 1. PE is the potential energy of the I structure in kJ/mol.

System		PE	Ring Size 3	4	5	6	7	8	9	10
ice I			0.0	0.0	0.0	720.0	0.0	0.0	0.0	0.0
A	1.27 GPa, 77 K	−51.0	4.2	45.4	108.7	160.8	49.5	1.9	0.0	0.0
B	0.0 GPa, 77 K	−52.1	2.8	38.0	132.6	159.8	40.5	2.1	0.0	0.0
C	1.27 GPa, 77 K	−51.5	2.5	34.8	96.9	119.2	55.6	3.0	0.0	0.0
D	0.0 GPa, 77 K	−52.2	0.0	32.5	119.8	136.5	54.3	4.9	6.0	0.2
E	−0.2 GPa, 77 K	−52.3	0.2	31.0	140.5	156.5	42.3	1.7	0.0	0.0
F	160 K, 1.17 g/cm^3	−50.3	0.2	28.5	129.4	164.5	43.0	1.0	0.0	0.0
G	−0.2 GPa, 160 K	−50.2	0.0	26.6	148.5	200.9	32.2	0.1	0.0	0.0
H	300 K, 1.00 g/cm^3	−50.8	2.1	30.7	79.4	95.0	44.9	7.0	0.5	0.0

This means that the ratio ξ_d is large (small) if the molecular displacements are localized (delocalized). When the distribution of ΔR is Gaussian, ξ_d is 5/3. The time dependence of the displacement moment ratio is shown in Fig. 3. Clearly seen is the difference in the magnitude of the moment ratio between transitions before and after the abrupt change of the density at about t=1200 ps. The moment ratio is small in the early stage of the relaxation. The number of water molecules involved in a single transition is approximately 20. After t=1200 ps, some large moment ratios are observed, which means localized displacements occur frequently. The latter half of the relaxation is comprised of a large number of localized motions accompanied by a small number of highly cooperative transitions. Most of the transitions are restricted to those motions involving few water molecules.

B. From HDA to LDA

An NPT simulation is performed for 800 ps at negative pressure -0.2 GPa and 77 K, which corresponds to those between state points C and E. After that, we perform an NVE simulation for 100 ps in order to compare the measurable quantities. The data for E are given by averaging 1000 configurations during the NVE simulation. After the system E is heated up to 160 K, an NVT simulation is performed for 650 ps and an NVE simulation is continued for 500 ps. The data for G are given from 1000 configurations in the last 100 ps of the NVE simulation. We consider E (G) as the representative structures as HDA (LDA). We also obtain the systems F and H. H is given by averaging 1000 configurations in 100 ps NVE simulation at 300 K and 1.00 g/cm^3. F is given by heating system E (HDA) to 160 K without changing density. It takes 280 ps of NVT simulation and 425 ps of NVE simulation to reach equilibrium. The data for F are given by the average of 1000 configurations in the

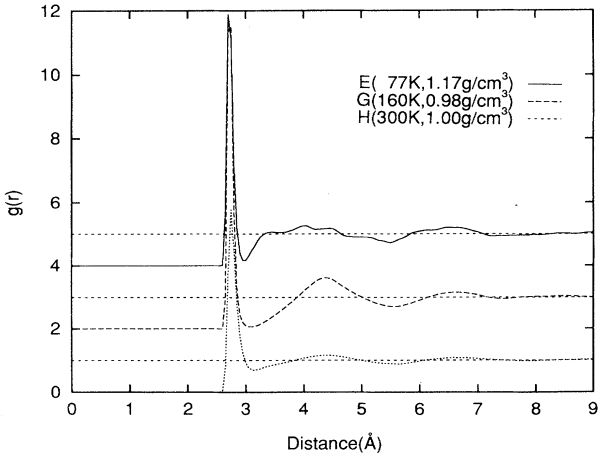

FIG. 4. Radial distribution functions (O—O) for the V structure of water in systems E (HDA, solid line), G (LDA, dashed line), and H (liquid water, dotted line).

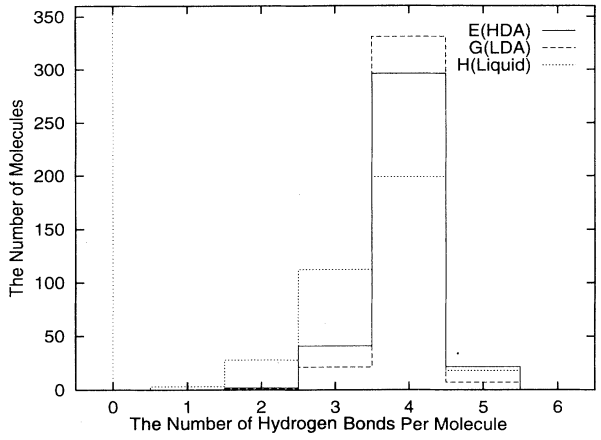

FIG. 5. The number of hydrogen bonds per molecule in V structure in systems E (HDA, solid line), G (LDA, dashed line), and H (liquid water, dotted line).

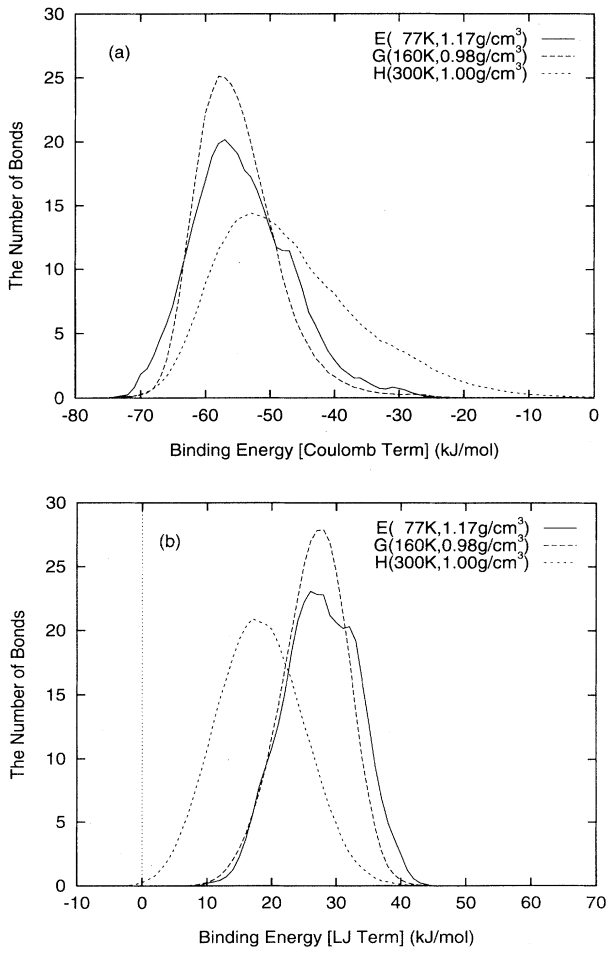

FIG. 6. Distributions of binding energy in systems E (HDA, solid line), G (LDA, dashed line), and H (liquid water, dotted line). These distributions are only for pairs whose distances are less than 3.5 Å. (a) is for the Coulomb term and (b) is for the LJ term.

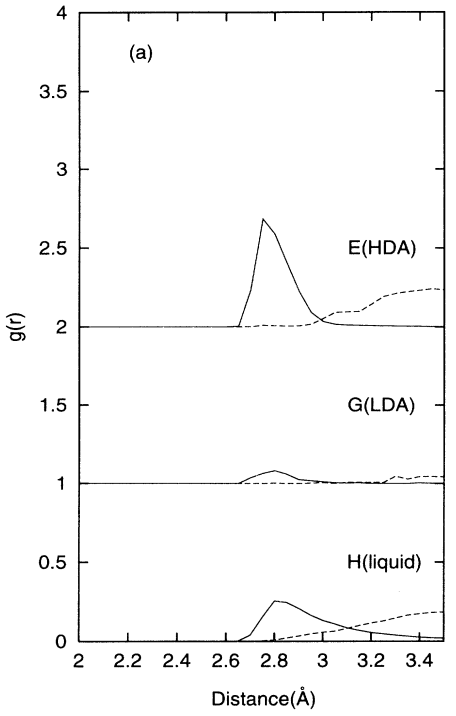

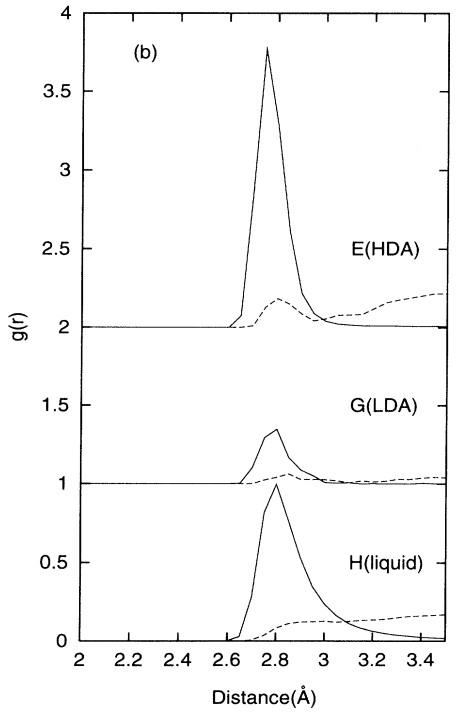

FIG. 7. Radial distribution functions for the bifurcated bonds. (a) Distribution for BB_H. Solid line is for the strongest bond in a pair of bifurcated bonds. Dashed line is for the second or third strongest bond. (b) Distribution for BB_O. Solid line is for the first and second strongest bond in a pair of bifurcated bonds. Dashed line is for the third or fourth strongest bond. The meaning of BB_H and BB_O is shown in the text.

last 100 ps NVE simulation.

Ice I_h is experimentally the most stable phase at the condition of F In the simulation, however, transformation to ice I_h cannot be observed because it takes a much longer time than the time scale of ordinary simulation for a nucleus to extend the entire simulation cell. Therefore, the system remains a metastable state.

The structure of LDA resembles that of ice I_h in short range order more than HDA. The first piece of evidence for this is the RDF. Figure 4 shows RDF for the V structure of HDA, LDA, and liquid water at 300 K. The peak positions do not differ from each other. On the other hand, there is a large difference in the height of the second peak. The second peak for LDA is clearly separated from the first one by a deep well. On the contrary, the second peak for HDA is split and separation from the first peak is not so distinct as that of LDA. In the case of liquid water, the first minimum is very shallow. The distribution of the number of hydrogen bonds per molecule in the V structure is shown in Fig. 5. More than 80% of the molecules have four hydrogen bonds in HDA and LDA. On the other hand, the number of molecules with four hydrogen bonds in liquid water is less than 60%. The number of four intact hydrogen bonds is the greatest in LDA. The binding energy distribution also supports the above view. Figures 6(a) and 6(b) show the binding energy distribution functions of the Coulomb part and Lennard-Jones (LJ) part for E (HDA), G (LDA), and H (liquid water). The peak of the distribution of the LJ part of the binding energy in LDA is higher than that in liquid water at 300 K. The number of molecules whose Coulomb energy $|E_c|$ is smaller than 48 kJ/mol decreases more in LDA than in HDA and in liquid water. In the region of $|E_c| > 48$ kJ/mol, however, the reverse holds. This results from the fact that orientations are dominated by the strong Coulombic interaction. Since the Coulombic interaction is so strong, the LJ part of the interaction,

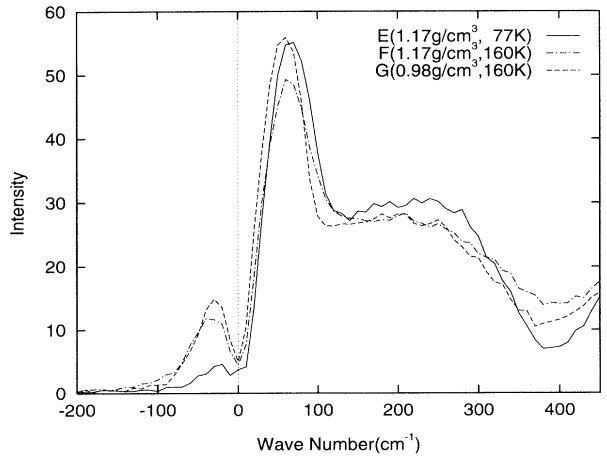

FIG. 8. Density of state for intermolecular vibrational motions for water in systems E (HDA, solid line), F (dash-dot line), and G (LDA, dashed line).

which is not compatible with the Coulombic interaction, becomes repulsive. This is the second piece of evidence for structural similarity of LDA to ice I_h in short range order.

The third piece of evidence is obtained from the analysis of the bifurcated hydrogen bond and the ring structure. The RDF of two kinds of bifurcated bonds is presented in Fig. 7. The number of BB_O is larger than that of BB_H. This is partly due to the functional form of the intermolecular interaction: Since only a single site with negative charge exists on C_{2v} bisector in TIP4P potential, the potential energy around an oxygen atom does not change so harshly as that around a hydrogen atom. The number of the bifurcated bonds is the largest in HDA whereas that in LDA is much less than in HDA and liquid state. Figure 7 shows that most of the bifurcated bonds are originated from an oxygen atom in both the first and the second coordination shell. In liquid water and HDA, we observe BB_O, which consists of two molecules in the first coordination shell. Only liquid water has BB_H, which consists of two molecules in the first coordination shell. On the other hand, there are few bifurcated bonds in LDA. According to the distribution of ring size, the concentrations of 5- and 6-membered rings in LDA and HDA are much more populated than those in liquid water, whereas the concentration of 7-membered rings is much less than that in liquid water. This is enhanced especially in LDA, where the number of linear hydrogen bonds is larger than that in water and in HDA.

In order to see how the vibrational modes are delocalized in space, the moment ratio of each eigenvector is calculated, which is defined as

$$\xi_e = \frac{\frac{1}{N_f}\sum_i e_i^4}{\left(\frac{1}{N_f}\sum_i e_i^2\right)^2} \qquad (6)$$

Here $\boldsymbol{e}$ is the corresponding individual molecular displacements of an eigenvector, and the average is taken over all molecules. ξ_e has the same property as ξ_d. In liquid water, there are a number of modes between 400 and 500 cm^{-1} (see Fig. 8). These modes are localized and their eigenvectors contain both translational and rotational elements [1]. Figure 9 shows the frequency dependence of ξ_e in the unstable (imaginary) frequency region. Increasing the temperature has two effects. One is to increase the number of unstable modes. Another is to decrease the mean moment ratio in the unstable region, which means that the number of delocalized modes increases. On the other hand, decreasing density does not change the number of unstable modes. The peak of $\rho(\omega)$ in LDA is more pronounced than in HDA and the localization of unstable modes is enhanced, especially below -30 cm^{-1}.

C. Density fluctuation in HDA and LDA

For the sake of examining density fluctuations in amorphous solids, an MD simulation is performed at 160 K and 1.08 g/cm^3 (system I) with a fixed volume. The density of the system lies between HDA and LDA. Since the system is probably unstable, we may observe the phase separation into the high density region and low density region.

In Fig. 10, the distributions of the volume of VPs for E (HDA), F, G, (LDA), H, and I are presented. Note that an oxygen atom has been considered as a center of the whole molecule. The distributions are broader in the lower density system (0.98 g/cm^3, 1.08 g/cm^3) than in higher density system (1.17 g/cm^3). No appreciable changes are found at different temperatures for higher density systems [E (HDA) and F]. The wide distribu-

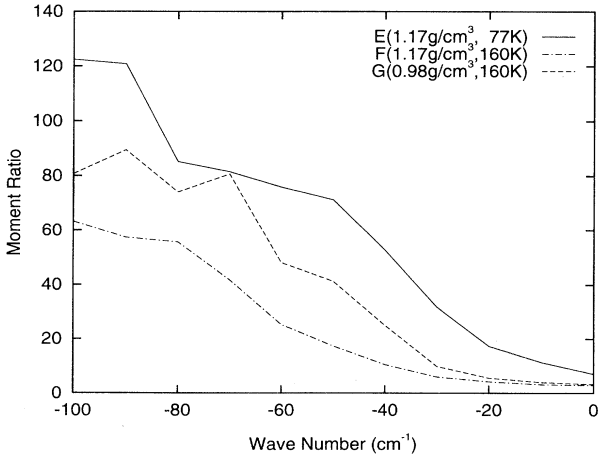

FIG. 9. Moment ratio ξ_e of the unstable modes in systems E (HDA, solid line), F (dash-dot line), and G (LDA, dashed line).

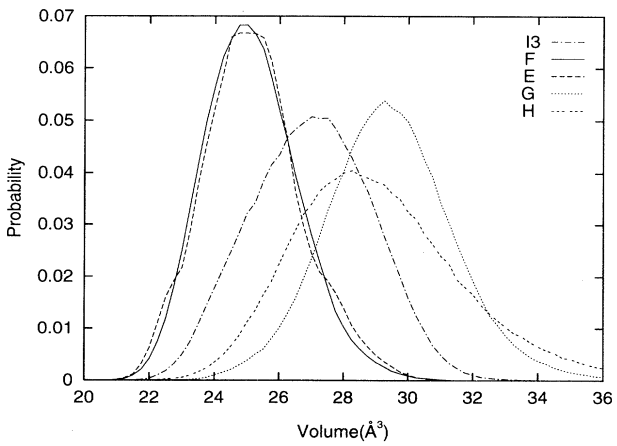

FIG. 10. Volume distributions of Voronoi polyhedra in systems E (dashed line), F (solid line), G (dotted line), H (thick dotted line), and I_3 (dash-dot line).

tion indicates that there are more distinctive states of individual water molecules in LDA than in HDA.

In order to see the spatial fluctuation of the amorphous ices, we calculate the static structure factor of molecules whose volumes of VPs are less than the average value. The structure factor is given by

$$\frac{1}{N_L}\left[\left(\sum_i \cos \boldsymbol{k}\cdot\boldsymbol{r}_i\right)^2+\left(\sum_i \sin \boldsymbol{k}\cdot\boldsymbol{r}_i\right)^2\right], \qquad (7)$$

where $\boldsymbol{r}_i$ is the position vector of the ith oxygen atom, and $\boldsymbol{k}$ is a wave vector. Note that the sum is taken over the molecules whose volumes of VPs are less than the average. N_L can be the number of those molecules, which belong to HDA phase. The structure factor thus defined is denoted by $S_v(k)$. If these selected molecules aggregate, the domain size becomes comparable to the system size and one can observe a peak in the small k region. This peak is a symptom of a phase separation. In Fig. 11, $S_v(k)$ for E (HDA), F, G (LDA), H, and I are shown. Large peaks appear in E (HDA), F, and I. The most important fact is that we can see peaks in the small wave number region even for E (HDA) and F. This is not observed when temperature goes up to 300 K at 1.0 g/cm^3, which ensures that the peak observed in E and F is not due to the thermal fluctuation but due to the precursor of phase separation. Comparing the position of the peak in low density region of $S_v(k)$, phase separation seems to cease in E. System E does not have enough kinetic energy to complete phase separation.

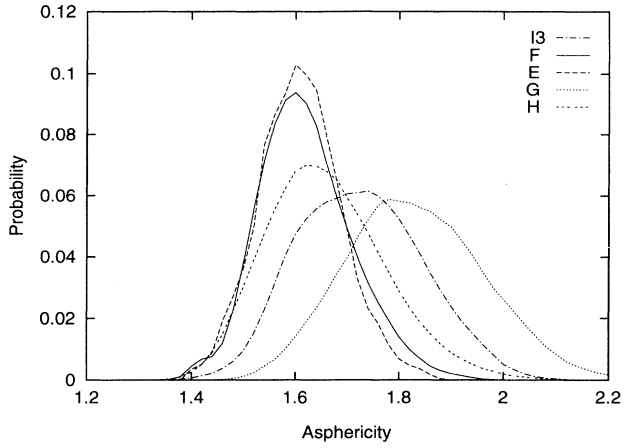

FIG. 12. Asphericity distributions of Voronoi polyhedra in systems E (dashed line), F (solid line), G (dotted line), H (thick dotted line), and I_3 (dash-dot line).

From the view point of the asphericity of VPs, we can see another picture of the structural fluctuation of amorphous ices. Figure 12 shows the asphericity distributions of VPs. In G or I, the distribution does not have a sharp peak but seems to be separated into two contributions. Another structure factor $S_a(k)$ is also calculated: the structure factor of the molecules whose asphericity is less than the average, which is shown in Fig. 13. In the case of E (LDA), the peak in the small wave number of $S_a(k)$

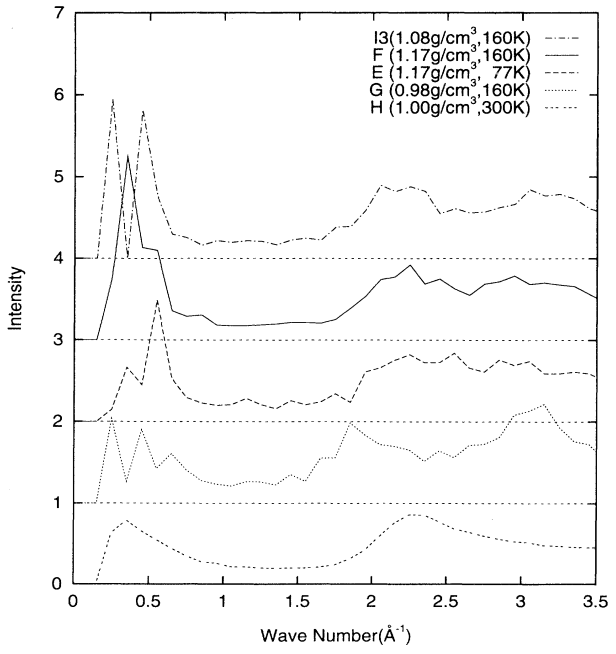

FIG. 11. Static structure factors $S_v(k)$ of the particles whose volume is smaller than average in systems E (dashed line), F (solid line), G (dotted line), H (thick dotted line), and I_3 (dash-dot line).

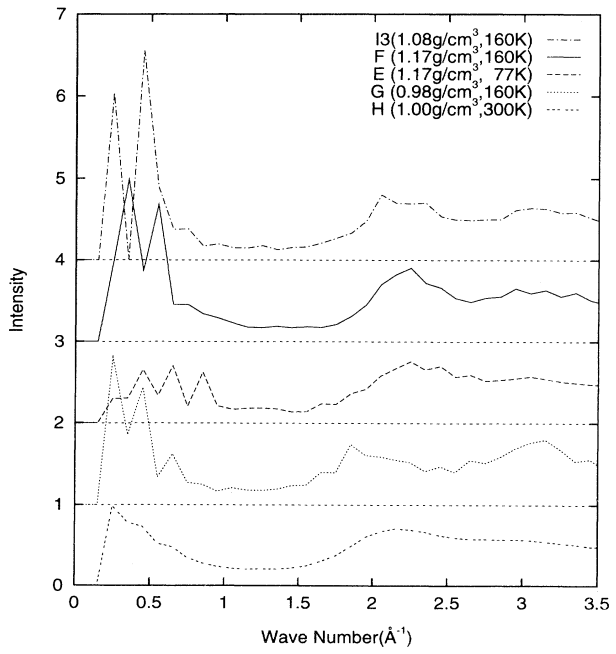

FIG. 13. Static structure factors $S_a(k)$ of the particles whose asphericity is smaller than average in systems E (dashed line), F (solid line), G (dotted line), H (thick dotted line), and I_3 (dash-dot line).

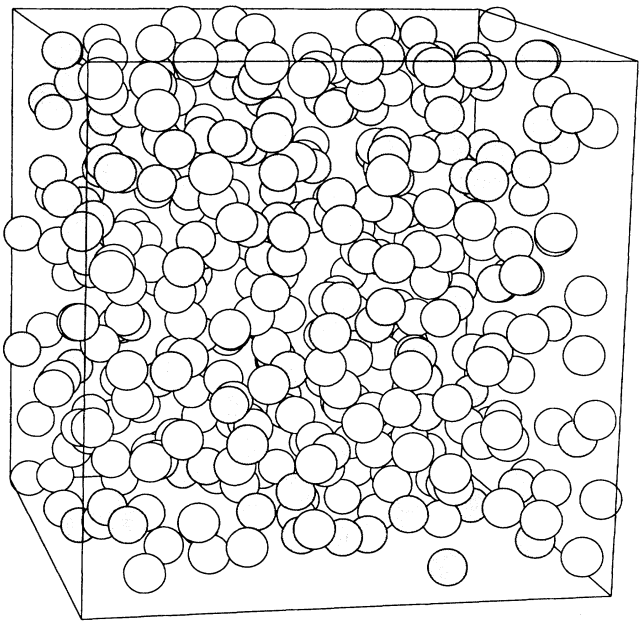

FIG. 14. Snapshot of the configuration at 1.08 g/cm^3 and 160 K. Water molecules are represented by spheres. Volumes of Voronoi polyhedra of shaded spheres are smaller than the average.

is higher than that of $S_v(k)$ as shown in Fig. 11. This indicates that the molecules, whose shapes are similar, tend to aggregate in LDA. This is not the case for HDA. In the case of I, both $S_v(k)$ and $S_a(k)$ have large peaks in the small wave number region (see Fig. 11). We can also observe the separation from the snapshot of system I (t=800 ps) shown in Fig. 14. This topological fluctuation may be associated with the spatial fluctuation proposed by Speedy [33,34].

IV. CONCLUDING REMARKS

Ice I_h transforms to high density amorphous phase (HDA) at 1.27 GPa and 77 K. However, since the low temperature does not allow a complete rearrangement of the local molecular configurations during compression, a simulation must be continued for about 3 ns after the transition in order to relax the system. The potential energy of the I structure of the system decreased by 0.5 kJ/mol during the slow relaxation. The numbers of 4-, 5-, and 6-membered rings decrease and those of 3-, 7-, and 8-membered rings increase during the relaxation. In the region after t=1200 ps the relaxation motions are more localized.

LDA is obtained by heating HDA to 160 K. The second peak of the RDF is more clearly separated from the first peak in LDA than in HDA. Few bifurcated bonds are found in LDA. These results mean that LDA resembles crystal ice more than HDA in short range order.

The network topology of the system is analyzed in terms of some distributions of VPs, where the density lies between stable HDA and LDA (1.08 g/cm^3). The static structure factor of the particles whose volume of VP is more than average is evaluated. It has a peak at small wave number, which suggests the phase separation into LDA and HDA begins to occur.

ACKNOWLEDGMENTS

The authors thank Professor X.C. Zeng for critical reading and helpful discussions. The present study was supported by a Grant-in-Aid from the Ministry of Education and Culture. Most of the computations have been made with the use of the supercomputer in the Computer Center in the Institute for Molecular Science and in the Institute for Chemical Research, Kyoto University.

[1] I. Ohmine and H. Tanaka, Chem. Rev. **93**, 2545 (1993).
[2] D. Eisenberg and W. Kauzmann, *The Structure and Properties of Water* (Oxford University, London, 1969).
[3] O. Mishima, L. D. Calvert, and E. Whalley, Nature **310**, 393 (1984).
[4] R. J. Speedy and C. A. Angell, J. Chem. Phys. **65**, 851 (1976).
[5] R. J. Speedy, J. Phys. Chem. **86**, 982 (1982); **86**, 3002 (1982); **91**, 3354 (1987).
[6] P. H. Poole, U. Essmann, F. Sciortino, and H. E. Stanley, Nature **360**, 324 (1992); P. H. Poole, F. Sciortino, U. Essmann, and H. E. Stanley, Phys. Rev. E **48**, 3799 (1993).
[7] P. H. Poole, F. Sciortino, T. Grande, H. E. Stanley, and C. A. Angell, Phys. Rev. Lett. **73**, 1632 (1994).
[8] M. G. Sceats and S. A. Rice, in *Water: A Comprehensive Treatise*, edited by F. Franks (Plenum, New York, 1982), Chap. 2.
[9] E. Mayer and P. Brüggeller, Nature **298**, 715 (1982).
[10] A. Kouchi and T. Kuroda, Nature **344**, 134 (1989).
[11] O. Mishima, L. D. Calvert, and E. Whalley, Nature **314**, 76 (1985).
[12] D. D. Klug, Y. P. Handa, J. S. Tse, and E. Whalley, J. Chem. Phys. **90**, 2390 (1989).
[13] O. Mishima, L. D. Calvert, and E. Whalley, Nature **314**, 76 (1985).
[14] O. Mishima, K. Takemura, and K. Aoki, Science **254**, 406 (1991); O. Mishima, J. Chem. Phys. **100**, 5910 (1994)
[15] H. M. Cohen and R. Roy, Phys. Chem. Glasses **6**, 149 (1965); W. Poch, *ibid.* **8**, 129 (1967).
[16] E. Whalley, D. D. Klug, and Y. P. Handa, Nature **342**, 782 (1989).
[17] M. A. Floriano, Y. P. Handa, D. D. Klug, and E. Whalley, J. Chem. Phys. **91**, 7187 (1989).
[18] D. D. Klug, O. Mishima, and E. Whalley, J. Chem. Phys. **86**, 5323 (1987).

[19] L. Bosio, G. P. Johari, and J. Teixeira, Phys. Rev. Lett. **56**, 460 (1986).
[20] J. S. Tse and M. L. Klein, Phys. Rev. Lett. **58**, 1672 (1987) ; J. S. Tse, in *Physics and Chemistry of Ice*, edited by M. Maeno and T. Hondoh (Hokkaido University Press, Sapporo, 1992), p. 91.
[21] P. H. Poole, U. Essmann, F. Sciortino, and H. E. Stanley, Phys. Rev. E **48**, 4605 (1993).
[22] H. E. Stanley, C. A. Angell, U. Essmann, M. Hemmati, P. H. Poole, and F. Sciortino, Physica A **205**, 122 (1994).
[23] J. D. Bernal and R. H. Fowler, J. Chem. Phys. **1**, 515 (1933).
[24] W. L. Jorgensen, J. Chandrasekhar, J. D. Madura, R. W. Impey, and M. L. Klein, J. Chem. Phys. **79**, 926 (1983).
[25] H. C. Andersen, J. Chem. Phys. **72**, 2384 (1980).
[26] S. Nosé, Mol. Phys. **52**, 255 (1984); J. Chem. Phys. **81**, 511 (1984); in *Computer Simulation in Materials Science*, edited by M. Mayer and V. Pontikis (Kluwer Academic Publishers, Dordrecht, 1991), p. 21.
[27] F. H. Stillinger and T. A. Weber, Phys. Rev. A **25**, 978 (1982).
[28] H. Tanaka and I. Ohmine, J. Chem. Phys. **87**, 6128 (1987).
[29] F. Hirata and P. J. Rossky, J. Chem. Phys. **74**, 6867 (1981).
[30] I. Ohmine, H. Tanaka, and P. G. Wolynes, J. Chem. Phys. **89**, 5852 (1988).
[31] G. Ruocco, M. Sampoli, and R. Vallauri, J. Chem. Phys. **96**, 6167 (1992).
[32] H. Tanaka and I. Ohmine, J. Chem. Phys. **91**, 6318 (1989).
[33] R. J. Speedy, J. Phys. Chem. **88**, 3364 (1984).
[34] R. J. Speedy and M. Mezei, J. Phys. Chem. **89**, 171 (1985).

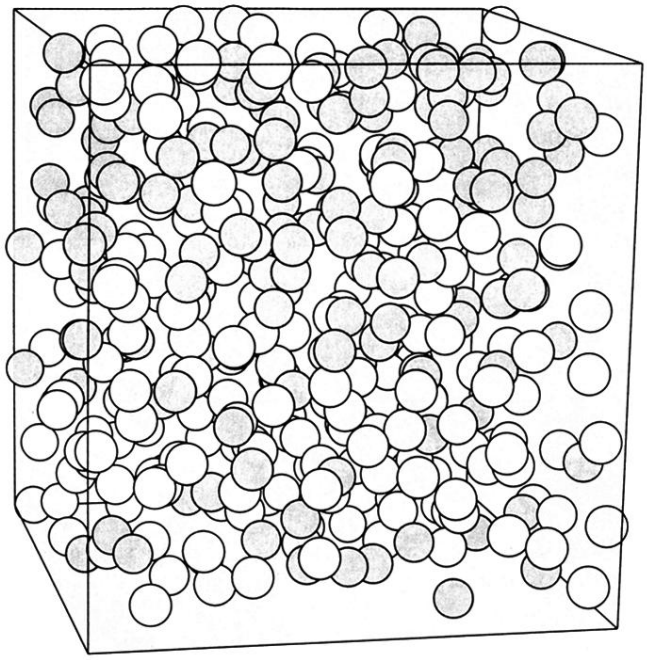

FIG. 14. Snapshot of the configuration at 1.08 g/cm^3 and 160 K. Water molecules are represented by spheres. Volumes of Voronoi polyhedra of shaded spheres are smaller than the average.